The QSO Luminosity Function from the 2dF QSO Redshift Survey and the Associated 6dF QSO Redshift Survey at $0.3 \leq z \leq 2.4$

Salam Ajitkumar Singh[1*] and K. Yugindro Singh[1]

Department of Physics, Manipur University, Canchipur, Imphal-795003, Manipur, India
Email: ajitkumarsalam@gmail.com

Abstract In this paper we present a determination of the optical luminosity function of Quasi Stellar Objects (QSOs) and its evolution, using data from the 2 Degree Field (2dF) QSO Redshift Survey (2QZ) and the associated 6 Degree Field (6dF) QSO Redshift Survey (6QZ) over the redshift range $0.3 \leq z \leq 2.4$ in a flat universe with $\Omega_{\rm m} = 0.3$ and $\Omega_{\Lambda} = 0.7$. The shape of the luminosity function is best fitted by a Schechter function model of the form $\Phi(L_{b_J})dL_{b_J} = \Phi^*(L_{b_J}/L^*_{b_J})^{\alpha} exp(-L_{b_J}/L^*_{b_J})d(L_{b_J}/L^*_{b_J})$, where $L^*_{b_J}$ is the break or characteristic luminosity. Using the Levenberg-Marquardt method of nonlinear least square fit we find the luminosity evolution model of the form $L^*_{b_J}(z) \propto 10^{1.56z-0.34z^2}$.

Keywords: galaxies:active, quasars:general.

1 Introduction

The most luminous Active Galactic Nuclei (AGNs), generally referred to as Quasi Stellar Objects (QSOs) or quasars, are fundamental to the study of galaxy evolution, intergalactic medium, large scale structure and cosmology. Soon after the discovery of QSOs, characterizing the QSO luminosity function and its evolution with redshift became an area of intense study [1,2]. The QSO luminosity function provides important information about the impact of QSO activity on the formation and evolution of the host galaxies [3,4]. It also provides one of the most important tools for the cosmic demography of AGNs and constraints on physical models and evolutionary theories of AGN [5,6,7].

The luminosity function is defined as the number of objects per unit comoving volume per unit luminosity as a function of luminosity and redshift [8,9]. In this paper, we find that the shape of the QSO luminosity function can be well represented by a Schechter function model [10]. In earlier papers such as Goldschmidt & Miller (1998) [11] and Warren et al. (1994) [12] the Schechtor function model is found to represent the shape of the QSO luminosity function. Using the Edinburgh UVX quasar survey, Goldschmidt & Miller (1998) used the Schechter function model with the evolution of the characteristic magnitude, $M^*(z) = M_0 - 2.5\gamma log_{10}(1+z)$ to fit the quasar luminosity function at the redshift range $1.7 \leq z \leq 2.2$. The fit is observed to be acceptable with a significance level for rejection of 10% and the best fitting parameter values are $\alpha = 1.7 \pm 0.3$, $M_0 = -23.7 \pm 0.4$ and $\gamma = 2.5 \pm 0.3$. Warren et al. (1994) used the Schechter function model with evolution of the characteristic magnitude of the form $M^*(z) = M_0 - 1.08k_L\tau$ using a wide-field multicolor survey for high redshift quasars ($z \geq 2.2$).

To describe the evolution of luminosity function with redshift, many models has been proposed. The most commonly used are the Pure Luminosity Evolution (PLE) [13] which assumes that only the luminosity of the QSOs changes with time but their number density remains constant and also the Pure Density Evolution (PDE) [13] in which only the number density of QSOs is changing with time but their luminosities remain constant. More complex models were also used to describe the evolution of luminosity function namely the Luminosity Dependent Density Evolution (LDDE) and the Luminosity Evolution and Density Evolution (LEDE). The LDDE describes the changes in the number density of QSOs allowing also for separate evolution between faint and bright objects [14]. The LEDE allows for evolution in luminosity and number density simultaneously [15]. The evolution of luminosity function derived from the 2QZ and 6QZ samples is well described by the PLE.

The plan of the paper is as follows. In section 2, we give a brief description of the 2QZ and 6QZ samples. The calculation of the binned optical luminosity function of QSOs and its analysis are presented in section 3 and our conclusions are given in section 4. Throughout this paper we assume a Λ cosmology with $\Omega_{\rm m} = 0.3$, $\Omega_\Lambda = 0.7$, and $H_o = 70.0$ km s^{-1} Mpc^{-1}.

2 The Data

For the study of QSO luminosity function we use the data taken from the 2 Degree Field (2dF) QSO Redshift Survey (2QZ) [16] and 6 Degree Field (6dF) QSO Redshift Survey (6QZ). Spectroscopic observations for the 2QZ and 6QZ were made with the 2dF instrument at the Anglo-Australian Telescope (AAT) [17] and the 6dF instrument at the United Kingdom Schmidth Telescope (UKST), respectively. The QSO candidates over the range $16.0 < b_J \leq 20.85$ for the 2QZ and 6QZ surveys are selected based on the broadband ub_Jr colours from automated plate measurement (APM) of UKST photographic plates. The 2QZ comprizes of 23,338 QSOs, 12,292 galactic stars (including 2,071 white dwarfs) and 4,558 compact narrow emission-line galaxies. In the 6QZ survey, there are 322 QSOs identified spectroscopically. The total survey area comprised 30 UKST fields, arranged in two $75^0 \times 5^0$ declination strips, one passing across the South Galactic Cap centered on Dec. $\delta = -30^0$ with RA range $\alpha = 21^h40^m$ to 3^h15^m (Known as the SGP strip, where SGP stands for 'South Galactic Pole') and the other across the North Galactic Cap centered on Dec. $\delta = 0^0$ with RA range $\alpha = 9^h50^m$ to 14^h50^m (Known as the NGP strip or the equatorial strip, where NGP stands for 'North Galactic Pole') [16,18,19,20,21]. Each strip is contiguous except for small regions around bright stars. These regions coincide with those of the 2dF Galaxy Redshift Survey (2dFGRS) [22], so that spectroscopic observations were carried out in collaboration with the galaxy survey. The survey was constructed in a B1950 coordinate system, although the publically available catalog is presented with J2000 positions. The total survey area is 721.6 deg^2, when allowance is made for regions of sky excised around the bright stars. The QSO candidates for the 2QZ ($18.25 < b_J < 20.85$) were selected based on fulfilling at least one of the following colour criteria: $u - b_J \leq -0.36$; $u - b_J < -0.12 - 0.8(b_J - r)$; $b_J - r < 0.05$ [7,18,19] and for the 6QZ ($16.0 < b_J < 18.25$) the colour criteria is $u - b_J \leq -0.50$ [18,23]. The data from both the 2dF and 6dF were reduced using the pipeline data reduction system 2DFDR [24]. Identification of spectra and the determination of redshifts of the QSO candidates were carried out by an automated program known as AUTOZ [16]. For the 2QZ and 6QZ surveys completeness, and sources of incompleteness, the four types of completeness i.e. morphological completeness, photometric completeness, coverage completeness (or coverage) and spectroscopic completeness are used (details are discussed in [18]).

3 The QSO Luminosity Function and Model Fits

In Figure 1, we show the absolute magnitude versus redshift distribution of the 2QZ and 6QZ QSOs. The histograms at the bottom and left of the figure show the one-dimensional distribution of QSOs in redshift and absolute magnitude, respectively. Using this samples, we calculate the binned luminosity function of QSOs by using the $1/V$ estimator devised by Page and Carrera (2000) [25] over the redshift range $0.3 \leq z \leq 2.4$.

The redshift ranges $0.3 \leq z \leq 2.4$ are divided into nine redshift bins. The edges of the redshift bins in which we calculate the luminosity function are: 0.3, 0.5, 0.7, 0.9, 1.1, 1.3, 1.5, 1.7, 1.9 and 2.4. The absolute magnitude bins are in increments of 0.3 mag. The binned luminosity function estimator of Page and Carrera [25] is given by

$$\Phi_{est} = \frac{N}{\int_{L_{min}}^{L_{max}} \int_{z_{min}}^{z_{max}(L)} \frac{dV}{dz} dz dL}, \tag{1}$$

where N is the number of objects of luminosity L found in comoving volume V at redshift z. The comoving volume is calculated by using a fixed, flat ($\Omega_{\rm m}$, Ω_Λ, H_o) = (0.3, 0.7, 70.0) universe, and the area of sample (721.6 deg^2). The resulting observed QSO luminosity functions from the samples is plotted in Figure 2.

The QSO luminosity function is traditionally fitted by a double power-law model in the literature [26,27,28,29]. However, in this paper the alternative model such as the Schechter function model [10] is

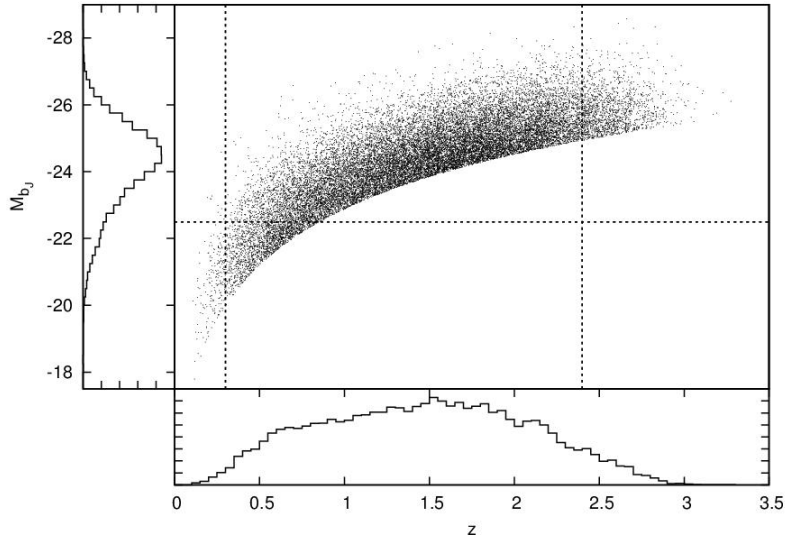

Figure 1. The distribution of the 2QZ and 6QZ QSOs in $z - M_{b_J}$ plane. The normalized redshift distributions of the samples are shown in the bottom panel and the normalized absolute magnitude in b_J-band are shown in the left panel of the figure. Dotted lines indicate the limits of our analysis i.e. $M_{b_J} < -22.5$ and $0.3 \leq z \leq 2.4$.

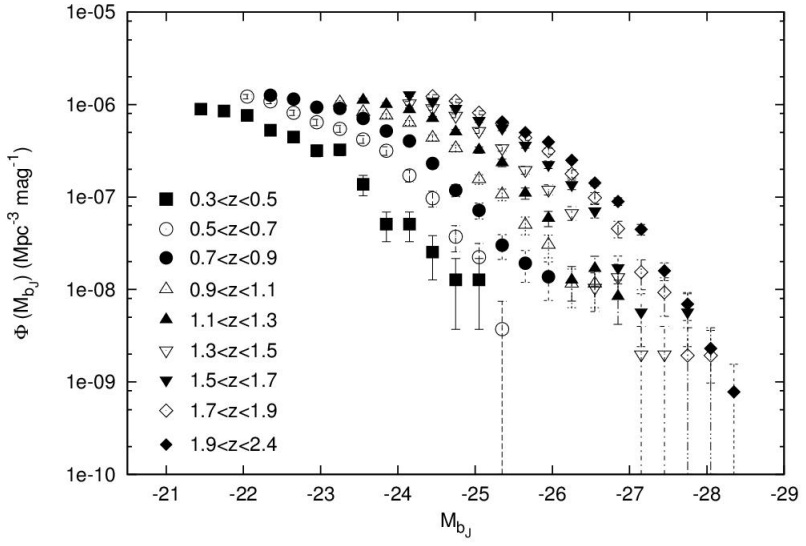

Figure 2. The observed luminosity function of QSOs over the redshift range $0.3 \leq z \leq 2.4$ determined from the 2QZ and 6QZ samples.

used to fit the QSO luminosity function. The generalized form of the Schechter function model is

$$\Phi(L_{b_J})dL_{b_J} = \Phi^*(L_{b_J}/L^*_{b_J})^{\alpha} exp(-L_{b_J}/L^*_{b_J})d(L_{b_J}/L^*_{b_J}),$$

which in terms of absolute magnitude becomes

$$\Phi(M_{b_J}) = 0.4ln(10)\Phi^* 10^{-0.4(M_{b_J}-M^*_{b_J})(\alpha+1)} \times exp[-10^{-0.4(M_{b_J}-M^*_{b_J})}], \quad (2)$$

where $L^*_{b_J}$ is the characteristic luminosity (with an equivalent characteristic absolute magnitude, $M^*_{b_J}$) and α is the faint-end slope of the luminosity. The evolution of luminosity function is given by the redshift dependence of the break luminosity, or break magnitude, which is chosen as second order polynomial in

redshift of the form

$$L^*_{b_J}(z) \equiv L^*_{b_J}(0)10^{k_1 z + k_2 z^2}.$$

In terms of absolute magnitude, this becomes

$$M^*_{b_J}(z) \equiv M^*_{b_J}(0) - 2.5(k_1 z + k_2 z^2). \quad (3)$$

We perform χ^2 fits to the binned data with five total free parameters (α, $M^*_{b_J}$, Φ^*, k_1, k_2) of the Schechter function model with PLE model, using the Levenberg-Marquardt method of nonlinear least square fit [30] to find the best fit parameters by minimizing the χ^2. The resulting fit to the observed luminosity function for the 2QZ and 6QZ samples over the redshift ranges $0.3 \leq z \leq 2.4$ with $M_{b_J} < -22.5$ is shown in Figure 3. In this figure, it is clear that there is in general good agreement between the model and data. However, there are more bright QSOs than the predicted by the model at the bright end of the luminosity function which is due to exponential decrease in the Schechter function model at $L_{b_J} >> L^*_{b_J}$. The resulting best fit parameter values for the Schechter function model with PLE are given in the first row of Table 1. In assessing the goodness-of-fit, we measure the χ^2 value by comparing the observed luminosity function and the theoretical luminosity function predicted by the best fit model. The resulting χ^2 value over the redshift range $0.3 \leq z \leq 2.4$ is $\chi^2/v = 174.39/98$ which means that the Schechter function model with PLE is significantly fit to the observed luminosity function of QSOs. For the purpose of comparison, the best fitting parameter values of Croom et al. (2004) [18], Croom et al. (2009) [31] and Ross et al. (2013) [29] are also provided in Table 1 and these values are consistent with our resulting parameters for the Schechter function model.

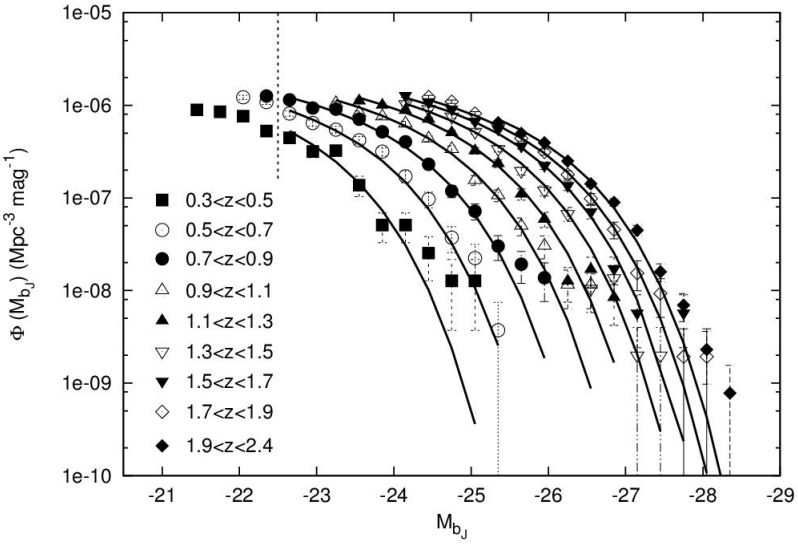

Figure 3. The Schechter function model fit to the observed luminosity function in nine redshift intervals over the redshift range $0.3 \leq z \leq 2.4$. The vertical dotted line gives a guide to the absolute magnitude limit, $M_{b_J} < -22.5$.

The number of QSOs in absolute magnitude bins of bin width=0.3 mag for the nine redshift ranges is predicted for the Schechter function model with polynomial evolution in a flat universe. The number of QSOs predicted (N_{pred}), observed (N_{obs}) and the significance of the difference between them (i.e. $\sigma = (N_{obs} - N_{pred})/\sqrt{N_{pred}}$) are given in Table 2. Negative value of σ means that there are more QSOs predicted than observed.

4 Conclusions

We have determined the luminosity function of QSOs and its evolution with redshift from the 2QZ and 6QZ samples in the b_J-band by using $1/V$ estimator devised by Page & Carrera over the redshift range

Table 1. The best fit parameter values for the Schechter function model with pure luminosity evolution (PLE) for the redshift range $0.3 \leq z \leq 2.4$ with $M_{b_J} < -22.5$ (in the first row).

Redshift Ranges	Models	β (Bright-end)	α (Faint-end)	$M^*_{b_J}$	k_1	k_2	$\Phi^* \times 10^{-06}$ (Mpc^{-3}mag^{-1})	χ^2/v	Reference
$0.3-2.4$	SF		-1.28	-21.43	1.56	-0.34	1.23	174.38/98	This paper
$0.4-2.1$	DPL	-3.29	-1.37	-22.09	1.44	-0.32	1.62	181.40/81	Croom et al. (2009)
$0.4-2.1$	DPL	-3.31	-1.09	-21.61	1.39	-0.29	1.67	71.10/62	Croom et al. (2004)
$1.06-2.2$	DPL	-3.55	-1.23	-22.92	1.29	-0.27	0.66	83.00/52	Ross et al. (2013)

DPL−double power-law model & SF−Schechter function model.

Table 2. The number of QSO observed (N_{pred}) and predicted (N_{pred}) from the Schechter function model with second order polynomial evolution for the redshift range $0.3 \leq z \leq 2.4$ with $M_{b_J} < -22.5$ in a flat universe.

$0.3 \leq z \leq 0.5$				$0.5 \leq z \leq 0.7$				$0.7 \leq z \leq 0.9$			
M_{b_J}	N_{obs}	N_{pre}	σ	M_{b_J}	N_{obs}	N_{pre}	σ	M_{b_J}	N_{obs}	N_{pre}	σ
-22.65	70	89.19	-2.03	-22.65	219	241.16	-1.42	-22.65	335	322.31	0.70
-22.95	50	65.96	-1.96	-22.95	173	196.20	-1.65	-22.95	339	380.16	-2.11
-23.25	51	49.27	0.24	-23.25	147	151.86	-0.39	-23.25	329	308.75	1.15
-23.54	16	30.29	-2.59	-23.55	113	108.31	0.45	-23.55	257	247.41	0.60
-23.85	8	16.60	-2.11	-23.85	85	73.84	1.29	-23.85	188	188.89	-0.06
-24.15	8	8.05	-0.02	-24.15	46	46.59	-0.08	-24.15	146	136.38	0.82
-24.45	4	3.28	0.39	-24.45	26	25.99	0.01	-24.45	84	88.14	-0.44
-24.75	2	0.35	2.73	-24.75	10	12.24	-0.64	-24.75	43	53.45	-1.42
-25.05	2	0.27	3.32	-25.05	6	3.56	1.28	-25.05	26	31.08	-0.91
–	–	–	–	-25.35	1	0.24	1.52	-25.35	11	10.25	0.23
–	–	–	–	–	–	–	–	-25.65	7	3.14	2.18
–	–	–	–	–	–	–	–	-25.95	5	2.04	2.06
$0.9 \leq z \leq 1.1$				$1.1 \leq z \leq 1.3$				$1.3 \leq z \leq 1.5$			
-23.25	453	490.74	-1.70	-23.55	446	449.84	-0.18	-24.15	528	527.80	0.01
-23.55	356	412.27	-2.77	-23.85	483	488.32	-0.24	-24.45	462	437.36	1.17
-23.85	324	337.19	-0.71	-24.15	418	404.78	0.65	-24.75	387	352.17	1.85
-24.15	275	263.45	0.71	-24.45	335	320.52	0.80	-25.05	263	260.49	0.15
-24.45	187	193.07	-0.43	-24.75	239	238.91	0.01	-25.35	171	185.32	-1.05
-24.75	144	136.07	0.67	-25.05	154	168.26	-1.09	-25.65	99	119.93	-1.91
-25.05	67	83.01	-1.75	-25.35	112	108.34	0.35	-25.95	61	73.87	-1.49
-25.35	46	47.88	-0.27	-25.65	53	65.66	-1.56	-26.25	34	35.98	-0.33
-25.65	21	21.54	-0.11	-25.95	28	34.82	-1.15	-26.55	5	14.98	-2.58
-25.95	13	9.81	1.01	-26.25	6	12.25	-1.78	-26.85	7	3.75	1.67
-26.25	5	2.52	1.56	-26.55	8	4.09	1.92	-27.15	1	0.70	0.34
-26.55	5	1.53	2.80	-26.85	4	2.62	0.85	-27.45	1	0.52	0.66
$1.5 \leq z \leq 1.7$				$1.7 \leq z \leq 1.9$				$1.9 \leq z \leq 2.4$			
-24.15	556	564.61	-0.36	-24.75	571	520.32	2.22	-25.05	1000	1072.93	-2.22
-24.45	569	523.51	1.98	-25.05	437	390.33	2.36	-25.35	835	916.38	-2.68
-24.75	475	444.19	1.46	-25.35	330	312.24	1.00	-25.65	653	697.56	-1.68
-25.05	357	344.02	0.69	-25.65	230	234.96	-0.32	-25.95	505	512.19	-0.31
-25.35	290	261.93	1.73	-25.95	168	159.45	0.67	-26.25	326	336.25	-0.55
-25.65	195	182.08	0.95	-26.25	94	97.23	-0.32	-26.54	183	191.22	-0.59
-25.95	115	119.21	-0.38	-26.55	54	54.34	-0.05	-26.85	116	100.16	1.58
-26.25	72	69.36	0.31	-26.85	24	24.28	-0.05	-27.15	58	44.12	2.08
-26.55	37	34.65	0.39	-27.15	8	9.49	-0.48	-27.45	21	15.21	1.48
-26.85	9	13.79	-1.29	-27.45	5	2.47	1.60	-27.75	9	3.68	2.76
-27.15	3	4.56	-0.73	-27.75	1	0.52	0.66	-28.05	3	0.53	3.37
-27.75	3	1.02	2.04	-28.05	1	0.77	0.25	-28.35	1	0.56	0.59

$0.3 \leq z \leq 2.4$. The shape of the QSO luminosity functions and its evolution with redshift is adequately represented by the Schechter function model with second order polynomial evolution in redshift. The Schechter function model is regarded as one way of describing the shape of the QSO luminosity function which displays a steepening above a characteristic luminosity $L^*_{b_J}$ (or below a characteristic absolute magnitude $M^*_{b_J}$). The best fit values for total five free parameters for the Schechter function model are determined, which are given in Table 1, along with their derived χ^2 value and degree of freedom. The statistical errors on individual parameters are $\sigma(\Phi^*) = \pm 0.06 \times 10^{-06}$ Mpc^{-3}mag^{-1}, $\sigma(\alpha) = \pm 0.01$, $\sigma(M^*_{b_J}) = \pm 0.03$, $\sigma(k_1) = \pm 0.10$ and $\sigma(k_2) = \pm 0.04$.

Acknowledgments. The 2QZ and 6QZ are based on observations made with the Anglo-Australian Telescope and the UK Schmidt Telescope. We are greatly indebted to the staffs of Anglo-Australian Observatory.

One of the authors, Salam Ajitkumar Singh acknowledges the Indian Space Research Organization (ISRO), Department of Space, Government of India for providing a JRF under a RESPOND Project (ISRO/RES/2/385/2013-14).

References

1. J. L. Greenstein and T. A. Mathews, "Red-Shift of the Unusual Radio Sourse: 3C 48," *Nature*, vol. 197, pp. 1041–1042, 1963.
2. E. M. Burbidge, "Quasi-Stellar Objects," *Annual Reviews of Astronomy & Astrophysics*, vol. 5, pp. 399–452, 1967.
3. A. Cattaneo et al., "The role of black holes in galaxy formation and evolution," *Nature*, vol. 460, pp. 213–219, 2009.
4. A. C. Fabian, "Observational Evidence of Active Galactic Nuclei Feedback," *Annual Reviews of Astronomy & Astrophysics*, vol. 50, pp. 455–489, 2012.
5. R. J. Terlevich and B. J. Boyle, "Young ellipticals at high redshift," *Monthly Notices of the Royal Astronomical Society*, vol. 262, pp. 491–198, 1993.
6. M. G. Haehnelt and M. J. Rees, "The formation of nuclei in newly formed galaxies and the evolution of the quasar population," *Monthly Notices of the Royal Astronomical Society*, vol. 263, pp. 168–178, 1993.
7. B. J. Boyle et al., "The 2dF QSO Redshift Survey - I. The optical luminosity function of quasi-stellar objects," *Monthly Notices of the Royal Astronomical Society*, vol. 317, pp. 1014–1022, 2000.
8. X. Fan et al., "High-redshift quasars found in Sloan Digital Sky Survey commissioning data. IV. Luminosity function from the fall equatorial stripe sample," *The Astronomical Journal*, vol. 121, pp. 54–65, 2001.
9. L. Jiang et al., "A spectroscopic survey of faint quasars in the SDSS Deep Stripe. I. Preliminary results from the co-added catalog," *The Astronomical Journal*, vol. 131, pp. 2788–2800, 2006.
10. P. Schechter, "An analytic expression for the luminosity function for galaxies," *The Astrophysical Journal*, vol. 203, pp. 297–306, 1976.
11. P. Goldschmidt and L. Miller, "The UVX quasar optical luminosity function and its evolution," *Monthly Notices of the Royal Astronomical Society*, vol. 293, pp. 107–112, 1998.
12. S. J. Warren, P. C. Hewett, and P. S. Osmer, "A Wide-Field Multicolor Survey for high-redshift quasars $z \geq 2.2$. III. The Luminosity Function," *The Astrophysical Journal*, vol. 421, pp. 412–433, 1994.
13. M. Schmidt, "Space distribution and luminosity functions of Quasi-Stellar Radio Sources," *The Astrophysical Journal*, vol. 151, pp. 393, 1968.
14. T. Miyaji, G. Hasinger, and M. Schmidt, "Soft X-ray AGN luminosity function from ROSAT surveys," *The Astronomy & Astrophysics*, vol. 353, pp. 25–40, 2000.
15. J. Aird et al., "The evolution of the hard X-ray luminosity function of AGN," *Monthly Notices of the Royal Astronomical Society*, vol. 401, pp. 2531–2551, 2010.
16. S. M. Croom et al., "The 2dF QSO Redshift Survey-V. The 10k catalogue," *Monthly Notices of the Royal Astronomical Society*, vol. 322, pp. L29–L36, 2001.
17. I. J. Lewis et al., "The Anglo-Australian Observatory 2dF facility," *Monthly Notices of the Royal Astronomical Society*, vol. 333, pp. 279–298, 2002.
18. S. M. Croom et al., "The 2dF QSO Redshift Survey-XII. The spectroscopic catalogue and luminosity function," *Monthly Notices of the Royal Astronomical Society*, vol. 349, pp. 1397–1418, 2004.
19. R. J. Smith et al., "The 2dF QSO Redshift Survey-III. The Input Catalogue," *Monthly Notices of the Royal Astronomical Society*, vol. 359, pp. 57–72, 2005.

20. P. J. Outram et al., "The 2dF QSO Redshift Survey-XI. The QSO power spectrum," *Monthly Notices of the Royal Astronomical Society*, vol. 342, pp. 483–495, 2003.
21. J. da Ângela et al., "The 2dF QSO Redshift Survey-XV. Correlation analysis of redshift-space distortions," *Monthly Notices of the Royal Astronomical Society*, vol. 360, pp. 1040–1054, 2005.
22. M. Colless et al., "The 2dF Galaxy Redshift Survey: spectra and redshifts," *Monthly Notices of the Royal Astronomical Society*, vol. 328, pp. 1039–1063, 2001.
23. S. M. Croom et al., "The 2dF QSO Redshift Survey-XIV. Structure and evolution from the two-point correlation function," *Monthly Notices of the Royal Astronomical Society*, vol. 356, pp. 415–438, 2005.
24. J. Bailey and G. Glazebrook, "2dF User Manual, Anglo-Australian Observatory," 1999.
25. M. J. Page and F. J. Carrera, "An improved method of constructing binned luminosity functions," *Monthly Notices of the Royal Astronomical Society*, vol. 311, pp. 433–440, 2000.
26. B. J. Boyle, T. Shanks, and B. A. Peterson, "The evolution of optically selected QSOs-II," *Monthly Notices of the Royal Astronomical Society*, vol. 235, pp. 935–948, 1988.
27. G. T. Richards et al., "The 2dF-SDSS LRG and QSO (2SLAQ) Survey: the $z < 2.1$ quasar luminosity function from 5645 quasars to g=21.85," *Monthly Notices of the Royal Astronomical Society*, vol. 360, pp. 839–852, 2005.
28. E. Glikman et al., "The faint end of the quasar luminosity function at $z \sim 4$: Implications for ionization of the intergalactic medium and cosmic downsizing," *The Astrophysical Journal Letters*, vol. 728, pp. L26–L30, 2011.
29. N. P. Ross et al., "The SDSS-III baryon oscillation spectroscopic survey: The quasar luminosity function from data release nine," *The Astrophysical Journal*, vol. 773, pp. 14, 2013.
30. W. H. Press, S. A. Teukolsky, W. T. Vetterling, and B. P. Flannery, *Numerical Recipes in Fortran 77*, Cambridge University Press, Cambridge, 1992.
31. S. M. Croom et al., "The 2dF-SDSS LRG and QSO survey: the QSO luminosity function at $0.4 < z < 2.6$," *Monthly Notices of the Royal Astronomical Society*, vol. 399, pp. 1755-1772, 2009.

